Effects of ambient exposure on photoluminescence of Dion-Jacobson tin-based halide perovskite

Received 00th January 20xx,
Accepted 00th January 20xx

DOI: 10.1039/x0xx00000x

Wen Ting Sun,[a#] Zengshan Xing,[b#] Aleksandr Sergeev,[b] Yanling He,[a] Alan Man Ching Ng,[c] Kam Sing Wong,[b] Lidija Molčanov,[d] Jasminka Popović[d,*] and Aleksandra B. Djurišić[a,*]

Tin-based halide perovskite materials are of interest for light-emitting applications due to their broad yellow emission, but they are known to exhibit inferior stability compared to the lead-based perovskites due to tendency of Sn^{2+} to be readily oxidized. Here we investigated the ambient stability of a Dion-Jacobson tin bromide perovskite. We found that the optical properties of the samples were more significantly affected by the moisture rather than the ratio of Sn^{2+}/Sn^{4+}. The exposure to humidity resulted in changes in the ratio of 2D $HDASnBr_4$ and hydrated 1D HDA_3SnBr_8 phases (where HDA denotes hexane-1,6-diammonium), with initial increase (up to ~40 h) in luminescence attributed to increasing fraction of hydrated 1D phase which contributes to self-trapped exciton emission. With further exposure to humidity, the material starts to degrade resulting in reduced luminescence after ~40 h. The use of additives for the suppression of oxidation of Sn^{2+}, namely $SnCl_2$ and tetraethyl orthosilicate (TEOS), results in prolonging the lifetime of the samples (>260 h for thin films with additives, compared to 180 h for thin films without additives). However, the persistence of luminescence with increased time of ambient exposure in samples prepared with additives can be attributed to the changes in the evolution of phase composition (ratios of 2D and hydrated 1D phases) over time rather than suppressing the oxidation of Sn^{2+}.

[a.] *Department of Physics, The University of Hong Kong, Pokfulam Road, Hong Kong*
[b.] *Department of Physics, Hong Kong University of Science and Technology, Clearwater Bay, Hong Kong*
[c.] *Core Research Facility, Southern University of Science and Technology, No. 1088, Xueyuan Rd., Shenzhen, 518055, Guangdong, PR China.*
[d.] *Ruđer Bošković Institute, Bijenička 54, Zagreb, Croatia.*
* Corresponding authors:Jasminka Popović: jpopovic@irb.hr, Aleksandra B. Djurišić: dalek@hku.hk.
#These authors contributed equally.
Electronic Supplementary Information (ESI) available: Photos and PL spectra of HDASnBr4 powder, SEM images, XRD patterns, XPS spectra for different times of ambient air exposure. See DOI: 10.1039/x0xx00000x

Introduction

Tin-based halide perovskites have been extensively investigated as a lead-free alternative for a variety of applications, including solar cell and light emission applications.[1-9] The 2D/quasi-2D tin halide perovskites are particularly attractive for applications as phosphors,[1,3,5,7] as well as emitting layers for warm yellow,[2] red,[6,8] and near-infrared[9] light emitting diodes (LEDs). 2D tin-based perovskites generally exhibit superior light emitting properties compared to 3D counterparts, as they are more resistant to the oxidation of Sn^{2+} to Sn^{4+}.[6] Consequently, they also exhibit improved stability compared to 3D tin-based perovskites, which was attributed to slowing down the diffusion of oxygen into the perovskite.[6]

In general, major issue in stability of tin-based perovskites is the tendency of Sn^{2+} to readily get oxidized into Sn^{4+}.[10,11] This applies not only to ambient exposure, but even to small amount of oxygen in the glovebox[10] or oxidizing effects of solvent (dimethyl sulfoxide (DMSO)) used for film preparation.[12,13] Consequently, different approaches have been investigated for improving the stability of tin-based halide perovskites, such as various additives to improve film quality and hinder the oxidation of Sn^{2+},[10,14-25] and protecting the exposed surface with protective surface layer.[11] Among various additives, tin halides and various reducing agents and/or antioxidant compounds have been very common. However, the majority of these additives have been investigated for 3D perovskites and solar cell applications. As 2D tin halide perovskites are more stable compared to their 3D counterparts,[10] it is of interest to investigate the effects of different additives on their long term stability with ambient exposure. We can distinguish two types of 2D halide perovskites, namely Ruddlesden-Popper (RP) and Dion-Jacobson (DJ).[1,26] RP perovskites incorporate a bilayer of monovalent spacer cations which separates layers of inorganic metal halide octahedra, which are typically offset by half a unit cell in in-plane direction.[26] DJ perovskites incorporate diammonium cations which are bound by hydrogen bonds to the layers of inorganic metal halide octahedra and exhibit no offset of inorganic layers.[26] Different 2D (single layers of inorganic tin halide octahedral separated by spacer cations) and quasi-2D (multiple layers of inorganic tin halide octahedral separated by spacer cations) tin halide perovskites have been reported to date,[1-3,5-8,17,22,27-34] including both RP[1,2,6-8,17,22,30,34] and DJ[3,5,27-33] perovskite materials. In general, these materials exhibit improved stability compared to 3D tin-based perovskites.[10] For example, it has been shown that they do not need to be synthesized in an inert atmosphere,[1,7] and they can exhibit ambient stability over a long period of time, which in the case of DJ octyldiammonium (ODA) perovskite exceeds 30 days.[32] However, stability of these materials in thin film form, which is relevant for device applications, is considerably lower. For example, while 2D RP film exhibited significantly improved stability compared to 3D counterpart, the relative absorbance still exhibited >10% decrease within 30 mins.[6] While the use of additives can be an effective way to improve thin film stability of tin halide perovskites,[18,35-39] the investigations of additives in 2D perovskites have been scarce.[10,17,22] In particular, DJ perovskites exhibit improved stability compared to RP ones, due to the absence of weak van der Waals interactions present in RP materials. Thus, possible method to achieve improved thin film stability is to select a Dion-Jacobson 2D tin halide perovskite with good stability, which can then be further enhanced by incorporation of additives.

Therefore, here we used hexane-1,6,diammonium (HDA) as spacer cations since it was reported that it yields tin-based bromide perovskite powder exhibiting excellent stability and bright light emission.[5] The reported structure is a solvate containing 1D perovskite described with the formula $HDA_3SnBr_8(CH_2Cl_2)$. Since the structure of 2D DJ tin-based perovskite with HDA spacer is not reported in the literature, our intention was to investigate the possibility of preparation of 2D material as well as to elucidate the impact of ambient exposure on photoluminescence properties. We have prepared polycrystalline samples in powder form and found them to be exceptionally stable, exhibiting bright yellow luminescence after a week of storage in ambient, as shown in **Figure S1**, Supplementary Information. The light emitting properties exhibited humidity-dependent changes during aging in ambient air, as shown in **Figures S2** and **S3**, i.e. the luminance decreased faster at higher humidity, while at lower humidity (30-40%) for a period of time an increase in photoluminescence was observed. The PLQY of freshly prepared powder samples was 59.2% (280 nm excitation)/ 67.7% (316 nm excitation).

Samples were also prepared in the form of thin films. Thin films exhibit lower stability due to increased paths for oxygen and moisture ingress through grain boundaries. Thus, they would exhibit observable changes over much shorter timescales compared to powder samples, which makes them convenient for this investigation. Therefore, we investigated the degradation process and possible methods to improve the stability on thin film samples. First, we optimized the solvent composition to minimize the content of DMSO while maintaining the film quality, since it is known that DMSO can result in the oxidation of Sn^{2+} but it also suppresses rapid crystallization,[12,13] and that film quality affects the penetration of oxygen and moisture and hence its long term stability.[10] Then, we investigated the use of different additives for suppressing Sn^{2+} oxidation. Among various additives, tin halides are commonly used and have yielded promising results.[10,14,15,35-37] Sn(0) nanoparticles have also been effective in suppressing Sn^{2+} oxidation.[38,39] While SnF_2 has been demonstrated to be very successful in suppressing oxidation of Sn^{2+},[35,37] we have observed a strong humidity dependence of the sample stability. Thus, among different potential additives, $SnCl_2$ is particularly interesting as it can function as a reducing agent[14] as well as a desiccant.[10] It also has high solubility in DMF[14] and it can act in synergy with antioxidant additives to further enhance the device stability.[10,18,24] Tetraethyl orthosilicate (TEOS) is another additive which has the potential to absorb the moisture at grain boundaries,[40] as well as act as oxygen scavenger.[41] Therefore, we investigated the addition of $SnCl_2$, TEOS, and their combination to $HDASnBr_4$ films and examined their long term stability in ambient. We found that $SnCl_2$ only and the combination of both additives resulted in improved stability of the films compared to TEOS only and films without additives. The film lifetime was similar for $SnCl_2$ only samples and $SnCl_2$+TEOS, while the oxidation of Sn^{2+} was effectively suppressed only in $SnCl_2$+TEOS samples. The changes in the film optical properties can be attributed to structural transformations upon exposure to moisture, which at first enhances the luminescence but ultimately leads to film degradation.

Results and Discussion

Photoluminescence spectra of $HDASnBr_4$ thin films prepared from different solvent as a function of ambient exposure duration are shown in **Figure 1a-c**.

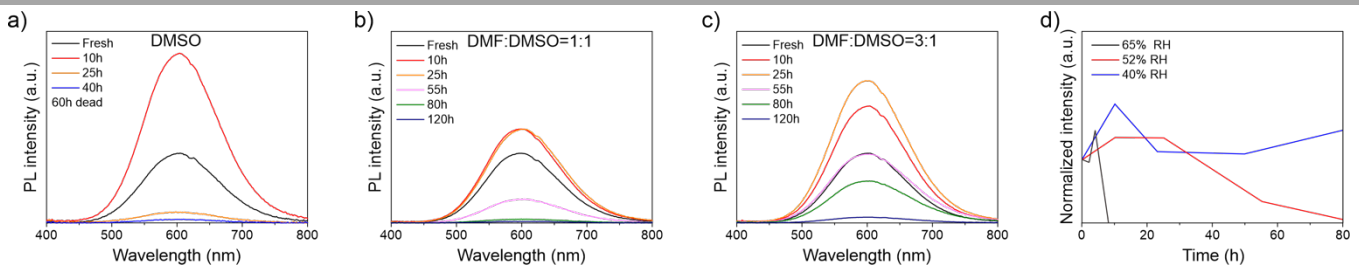

Figure 1. PL spectra of $HDASnBr_4$ prepared using different solvent and exposed to ambient air (RH ~50-55%) a) DMSO, b) DMF:DMSO 1:1 and c) DMF:DMSO 3:1; d) Normalized PL intensity of $HDASnBr_4$ (DMF:DMSO 1:1) as a function of time for different relative humidity levels.

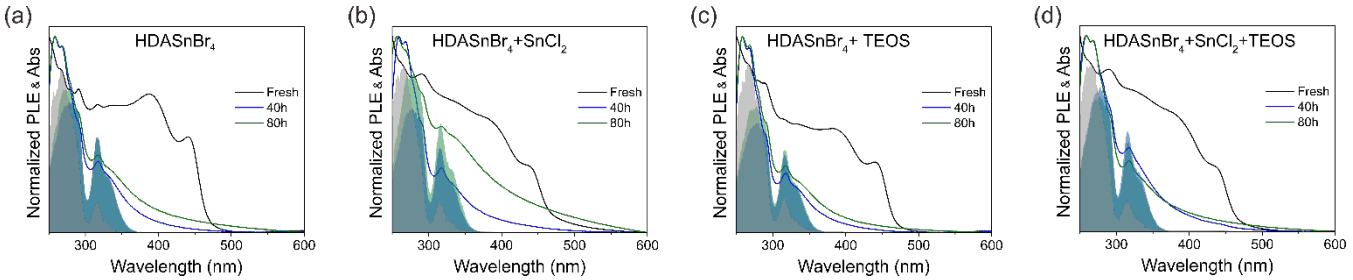

Figure 2. Normalized absorption (solid lines) and PLE (shaded areas) spectra of $HDASnBr_4$ samples with different additives: a) no additive, b) 10%$SnCl_2$, c) 7.5%TEOS, and d) $SnCl_2$+TEOS for different times of ambient exposure. Films were prepared in DMF:DMSO=3:1, and exposed to ambient atmosphere with RH in the range of ~32-40%. PLE spectra intensity was scaled to match the absorption in the range 280-290 nm.

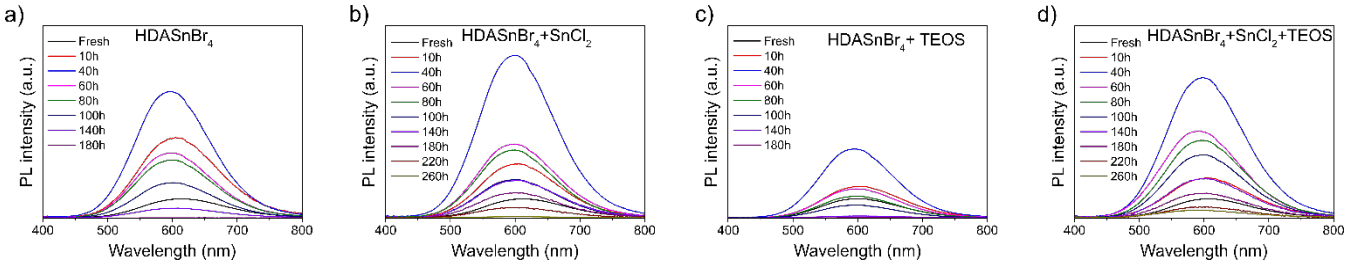

Figure 3. PL spectra of $HDASnBr_4$ samples with different additives: a) no additive, b) 10%$SnCl_2$, c) 7.5%TEOS, and d) $SnCl_2$+TEOS for different times of ambient exposure. Films were prepared in DMF:DMSO=3:1, and exposed to ambient atmosphere with RH in the range of ~32-40%.

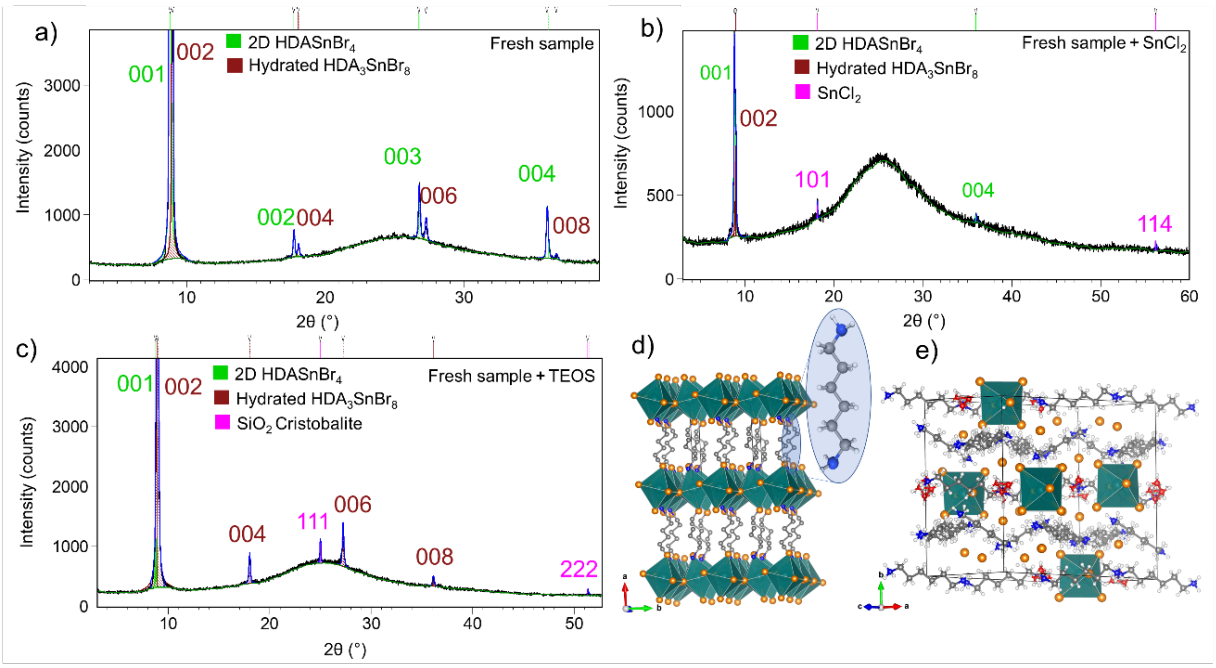

Figure 4. XRD patterns of fresh sample a) without additive and fresh samples with b) $SnCl_2$ and c) TEOS additives. Measured intensities are given by black dots while the calculated pattern is shown by blue line. d) Structure of 2D $HDASnBr_4$ phase, e) structure of 1D $HDA_3SnBr_8{\cdot}(H_2O)$ phase.

All the films exhibit characteristic broad emission which is attributed to self-trapped excitons (STE).[1-3,5] The STE occur due to transient lattice distortions upon photoexcitation and carrier-phonon coupling.[1,3] We can observe that lower DMSO content is associated with improved film stability, as expected, since the use of DMSO results in the oxidation of Sn^{2+} to Sn^{4+} in the precursor solution.[12,13] We can also observe that the film degradation exhibits significant dependence on relative humidity, with higher humidity levels leading to faster degradation, as shown in **Figure 1 d.** In all cases, we can observe first an increase in PL intensity, followed by a decrease. It is known that 2D perovskites, both DJ Pb-based[42] and RP Sn-based[43] can exhibit structural transformations upon exposure to humidity and/or solvent. Thus, although the effects of ambient exposure on optical properties of $HDASnBr_4$ are expected, it needs to be established whether humidity-induced transformations or the oxidation of Sn^{2+} play a larger role in the observed change of the optical properties. **Figures 2** and **3** show the PLE, absorption, and PL spectra, respectively, of $HDASnBr_4$ samples prepared from DMF:DMSO=3:1 with different additives. We can observe that all samples at first exhibit an increase (up to 40 h), followed by a decrease in the emission intensity, as shown in **Figure S4**. The samples containing $SnCl_2$ additive and samples containing both $SnCl_2$ and TEOS exhibit light emission for the longest period of time. Optical absorption spectra of Fresh and short-aged (10 h) samples contain two pronounced absorption bands centered around 400 and 450 nm (**Fig. 2** and **Fig. S5**) that could be attributed to intrinsic absorption of 2D $HDASnBr_4$ phase. At the same time, PLE spectra demonstrate no contribution of these bands to emission. That is evident from the flat PLE spectra in the 375-450 nm range for the Fresh and 10 h samples. The PLE spectra demonstrate a two-band structure with maxima at 280 and 316 nm. The position of these bands does not significantly change during aging, while the ratio of their intensities ($I(PLE_{280}):I(PLE_{316})$) decreases from 1:0.2 to 1:0.75 (**Fig S5**). Both PLE bands give a broadband PL (**Fig. 3**) with a large Stokes shift (>1.85 eV), indicating the STE emission, usual for these kinds of low-dimensional structures.[1-3,5] We can also observe that the absorption spectra exhibit a significant change in the shape of the absorption spectra around 40 h. Similar changes (shift of near-band edge absorption to shorter wavelength) were also observed due to dimensionality reduction of 2D lead-based DJ perovskite upon hydration.[42] In the morphology of the films, as shown in **Figure S6**, we can observe an appearance of needle-shaped grains around 40 h and the film roughness continues to increase with the time of ambient exposure, which is the likely reason for increased scattering in the absorption spectra of the samples. The observed changes in the morphology and absorption likely indicate structural changes, which cannot be distinguished from the photoluminescence spectra where broad yellow emission of varying intensity is observed in all cases. Nevertheless, phase transformations could cause variations in the emission intensity. For example, the emission spectra (peak position) and emission intensity in DJ tin halide perovskites were found to be dependent on the synthesis method,[5] possibly due to impurities and/or residual solvent molecules incorporated in the lattice.[5,31,32] In addition, it was previously reported that RP-based tin iodide perovskites could crystallize in dark and bright phases, which were both 2D phases, with somewhat larger spacing (<10% difference) observed in the bright phase.[1] It was proposed that bright phase had excess spacer cation and excess iodide, compared to stoichiometric dark phase.[1]

The XRD structural analysis was performed to identify the crystalline phases present in the samples and to investigate possible structural changes as a function of aging in ambient. *Le Bail* fit of fresh sample without additives and fresh samples containing $SnCl_2$, TEOS and a combination of $SnCl_2$+TEOS additives are shown in **Figure 4**. We can observe that all samples contain 2D phase $HDASnBr_4$ and 1D hydrate phase $HDA_3SnBr_8{\cdot}(H_2O)$. The structure of $HDAPbBr_4$ as reported by Terzis *et al.*,[44] was used as a starting structural model for the refinement of $HDASnBr_4$. The refinement showed that $HDASnBr_4$ crystalizes with periodicity along *c* direction of 11.89 Å, slightly smaller than reported value for $HDAPbBr_4$ (12.02 Å), which is in accordance with Sn^{2+} being smaller than Pb^{2+}. For the refinement of 1D phase, $HDA_3SnBr_8{\cdot}(H_2O)$ structure as reported by Ning *et al.* was used.[5] Besides perovskite phases, we can also observe the presence of crystalline phases belonging to additives; SiO_2 was refined by cubic F*d*-3*m* cristobalite structure deposited in Inorganic Crystal Structure Database under ICSD-77459, while $SnCl_2$ was refined by using the orthorhombic P*nma* structure (ICSD-81977). It is well known that various additives lead to improved perovskite performance and stability via several different mechanisms.[10] In some cases, the additive ions get incorporated within the perovskite lattice and therefore changes in structure on the molecular level are observed; this is often observed for hydrochloride containing additives that undergo halide exchange and mixed halide perovskite materials are formed.[45] In other cases, additive molecules, such as 5-ammonium valeric acid iodide, are attached *via* hydrogen bonds at the perovskite surface.[46] Finally, additives can also crystalize as a separate crystalline form,[36] usually at grain boundaries, as is the case in this our work. Both additives, TEOS and $SnCl_2$, have a similar underlaying mechanism by which the penetration of water molecules should be prevented or, at least, delayed. The $SnCl_2$ protective layer can acts as a desiccant agent due to the ability of $SnCl_2$ to absorb water molecules and form a stable hydrate ($SnCl_2{\cdot}2H_2O$) which can further on be oxidized to SnO_2.[10]

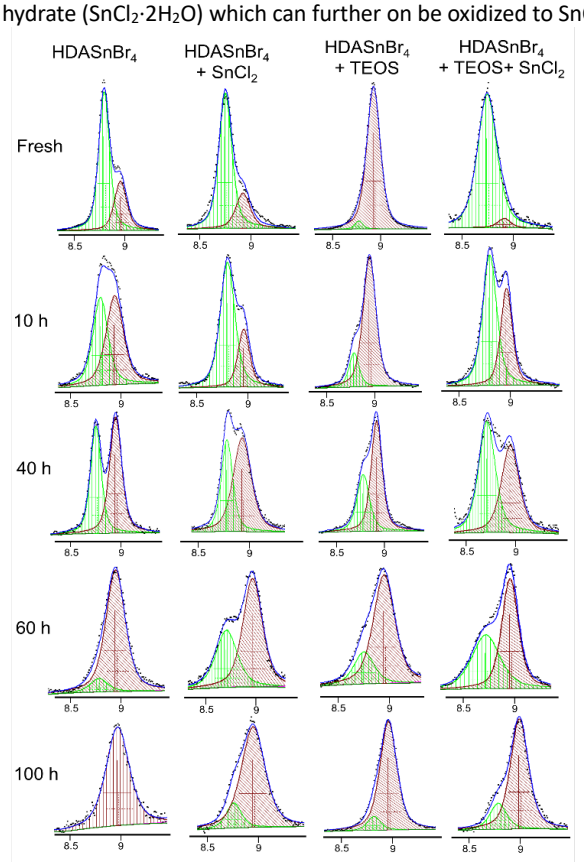

Figure 5 Small angle range of XRD patterns of sample without additive and samples with $SnCl_2$, TEOS, and $SnCl_2$+TEOS for different times of ambient exposure. Measured intensities are given by black dots while the calculated pattern is shown by blue line. 001 diffraction line of 2D perovskite is shown in green while the 002 line of hydrated 1D phase is given in dark red.

Similarly, water molecules can react with TEOS, forming SiO_2 and ethanol. Ethanol being volatile can readily escape, leaving the SiO_2 at the grain boundaries. Indeed, from **Figure 5.** we can observe that the amount of hydrated $HDA_3SnBr_8{\cdot}(H_2O)$ phase is smaller in fresh samples with $SnCl_2$ and TEOS+$SnCl_2$ additives, compared to the fresh sample without additives, pointing out that $SnCl_2$ efficiently absorbs water molecules and slows down the phase transformation from 2D phase to hydrated 1D phase. With exposure to ambient, the amount of hydrated 1D phase in all samples, with and without additives, is increasing. After 40 h of exposure, we can observe similar proportions of 2D and hydrated-1D phases. Interestingly, the samples with equal amounts of both phases are also exhibiting the highest PL intensity.

The efficiency of $SnCl_2$ and TEOS+$SnCl_2$ additives in slowing down the phase transformation from 2D phase to hydrated 1D phase is also obvious from 100 h aged samples; even after 100 h a considerable amount of 2D $HDASnBr_4$ phase is still preserved for samples with $SnCl_2$ and TEOS+$SnCl_2$ additives. The fact that 2D phase still exists in samples with $SnCl_2$ and TEOS+$SnCl_2$ additives, explains the prolongation of lifetime from 180 h to >260 h for thin films with additives. As the further discussion will show, the luminescence of all samples is attributed to the emission from the hydrated 1D phase. With aging in ambient, the crystallinity of luminescent 1D phase, in general, deteriorates. In the case of sample without additives, decreased crystallinity has a detrimental effect on optical properties, however the preservation of 2D phase due to the presence of $SnCl_2$ and TEOS+$SnCl_2$ additives enables the formation of new crystallites of 1D phase. Unlike additives that contain $SnCl_2$ (either pure $SnCl_2$ or the combination of TEOS+$SnCl_2$), sample with pure TEOS additive shows a different behavior. While all fresh samples dominantly contain 2D $HDASnBr_4$, the fresh sample with TEOS contains almost exclusively the hydrated 1D phase indicating on inferior desiccant efficacy compared to $SnCl_2$. The reason is too rapid reaction of TEOS with water molecules, yielding a SiO_2 phase probably simultaneously with the perovskite crystallization or even before it. Since all TEOS transformed to cristobalite even in fresh sample, the prolonged impact as desiccant agent is not likely. With aging, growth of the 2D $HDASnBr_4$ diffraction line is observed. This can possibly occur due to poor initial crystallinity of these samples, as shown in the SEM images (Figure S6). It is known that the exposure to moisture[47] or solvent vapor[48] can induce re-crystallization in halide perovskites, and this could explain an initial increase in $HDASnBr_4$ content in samples with TEOS. From the obtained results, it appears that ambient humidity plays a key role in the evolution of the optical properties and structure of $HDASnBr_4$ films. All XRD patterns of different samples as a function of time of ambient exposure are shown in **Figure S7**.

Due to known susceptibility of Sn^{2+} to oxidation, we have also performed XPS and examined the ratios of Sn^{2+}/Sn^{4+} in different samples as a function of time of ambient exposure. The obtained results are shown in **Figure 6** and **Figure S8**.

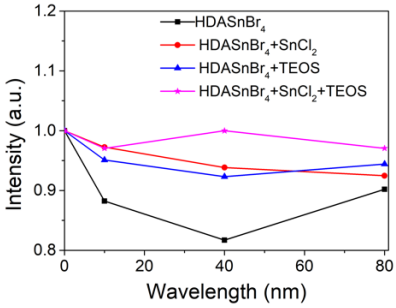

Figure 6. The normalized Sn^{2+}/Sn^{4+} ratio as a function of time of ambient exposure.

It should be noted that measurements are performed on different samples from the same batch, so that some sample-to-sample variation cannot be entirely excluded. Nevertheless, some clear trends can be observed. For example, we can observe that the lowest Sn^{2+}/Sn^{4+} ratio occurs at 40 h in all samples except the $HDASnBr_4$ + $SnCl_2$ + TEOS one. Although the samples with $SnCl_2$ and $SnCl_2$ + TEOS exhibit similar ambient stability (in terms of the time it takes of PL to decrease to zero), it appears that the samples with combined additives are more resistant to oxidation as the Sn^{2+}/Sn^{4+} remains practically unchanged over a period of time, while that ratio for samples with $SnCl_2$ only decreases. This can possibly be explained by different working mechanism of the two additives. As already mentioned $SnCl_2$ works as a desiccant and sacrificial material since it has the possibility to form a stable dihydrate which is then oxidized to SnO_2. This mechanism is supported by the appearance of SnO_2 diffraction lines in the XRD pattern of 100 h aged sample with $SnCl_2$ (**Figure S9**). Comparing the Sn^{2+}/Sn^{4+} ratios and PL intensity for different samples and different times of ambient exposure, no obvious correlation can be observed. Thus, we can conclude that the phase composition (the ratio of $HDASnBr_4$ phase and hydrated HDA_3SnBr_8) is the dominant factor affecting the photoluminescence intensity of the samples.

To investigate the reasons responsible for the observed behavior, more detailed investigation of the optical properties was performed. Since all samples exhibit the same optical properties, the following section will mainly discuss one of the samples ($HDASnBr_4$+TEOS). However, the suggestions made are also valid for other samples.

According to the phase composition, PLE bands originate from the hydrated HDA_3SnBr_8 phase appearing during the aging of the samples in the air. The aging process is accompanied by a gradual reduction of 2D $HDASnBr_4$ phase-related absorption peaks following by PL intensity increase. Starting from 40 hours aging, the absorption peaks at 400 and 450 nm became undistinguishable due to a transformation of 2D phase into hydrated one. That can be concluded from consistency between decreasing of 2D phase-related absorption peaks and increasing of hydrated phase-related PLQY (**Table 1**).

However, the PL decay traces show an inconsistent trend with the longest decay for the fresh sample and almost the same lifetime for the others (**Fig. 7**). Accounting for the well-known[49,50] relationship between PLQY, radiative (k_{rad}) and non-radiative ($k_{non\text{-}rad}$) rates

$$PLQY = \frac{k_{rad}}{k_{rad} + k_{non-rad}}$$

and assuming the number "dark" fraction (e.g., emission centers that absorbed photon but do not emit light within the period of measurement[51]) is constant, one can expect that shortening of PL decay time should result in lowering of PLQY. That inconsistence, together with changes in absorption spectra, from one side, and the same spectral profile of the PL, from the other side, suggest the different configurations of electronic states for the fresh and aged samples.

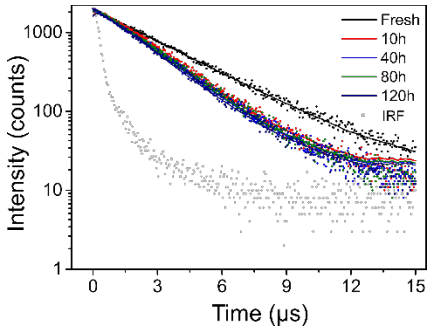

Figure 7. Changes in photoluminescence decay of the $HDASnBr_4$+TEOS sample during aging.

Table 1. PLQY data for the whole batch of the studied samples.

Sample	Aging time				
	Fresh	10 h	40 h	80 h	120 h
Excitation at 280 nm. PLQY, %					
Sample without additive	2.6	6.9	15.3	11.9	7.1
Sample with $SnCl_2$	2.2	3.8	14.7	10.7	8.6
Sample with TEOS	2.9	8.4	14.5	11.8	5.9
$HDASnBr_4$+ $SnCl_2$+TEOS	2.5	4.13	13.1	13	8.1
Excitation at 316 nm. PLQY, %					
$HDASnBr_4$	1.1	2.7	16.2	13.3	6.5
$HDASnBr_4$+$SnCl_2$	0.4	1.9	13.9	11.8	11.1
$HDASnBr_4$+TEOS	1.1	4.6	15.3	15	4
$HDASnBr_4$+ $SnCl_2$+TEOS	0.4	3.2	14.9	14.4	8.8

Combining the data presented in **Fig. 2, Fig. 3**, and **Fig. 7** we can propose the general model of STE emission regarding fresh and aged samples (**Fig. 8**).

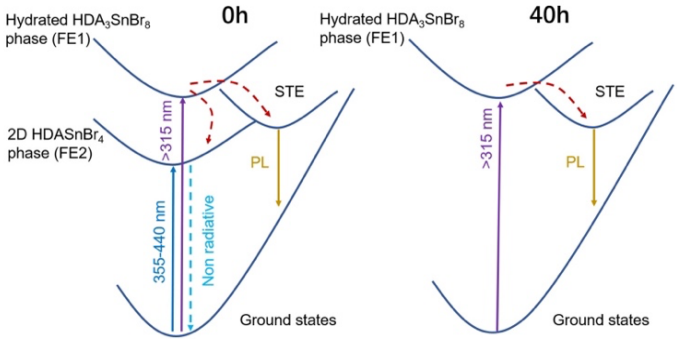

Figure 7. SET emission models of 0 h and 40 h samples.

Both fresh and aged samples have free exciton states (FE1) from the hydrated HDA_3SnBr_8 phase, concluded from the absorption peak at 316 nm. That absorption peak is consistent with the PLE peak, meaning that the free excitons generated in FE1 states under UV excitation, can further transform into an emissive STEs state. In addition, the excitonic absorption feature at around 450 nm in fresh samples can be attributed to the free exciton states (FE2) of the 2D phase. Also, most likely, the absorption band at 400 nm contributes to FE2 states as well. Thus, the absence of these absorption peaks in aged samples implies the absence of FE2 states. The FE2 states themselves provide a pathway for the non-radiative relaxation of free excitons from the FE1 states, competing the formation of the radiative STEs. Note that the free excitons from FE2 neither contribute to the STE emission as seen from the PLE spectra nor lead to free-exciton emission since no PL near the excitonic resonance at 450 nm has been detected. Finally, the free excitons at FE2 are not able to relax into the emissive STE states, probably due to the relatively larger potential barriers for the STE formation in the 2D phase.[49,52]

To verify that model, and get a deeper insight into the carriers' dynamics, transient absorption spectroscopy (TAS) studies were performed. The measurements were carried at two excitation wavelengths: 315 nm to evaluate the dynamics involved in the emission carriers and 415 nm to get an insight into carriers' dynamics within the 2D $HDASnBr_4$ phase, as shown in **Figure 9**.

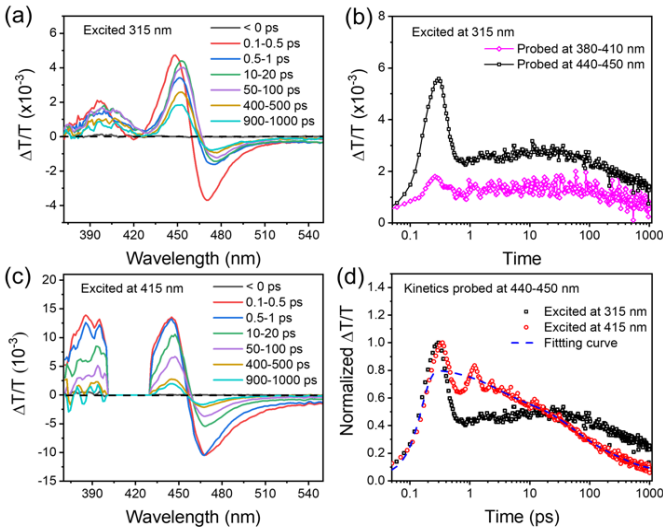

Figure 9. Transient absorption spectra of the fresh sample under 315 nm (a) and 415 nm (c) excitation; corresponding kinetics for PB1 and PB2 (b) under 315 nm excitation, and (d) comparison of PB2 kinetics for different excitation wavelengths.

The photobleaching (PB) signals at 400 nm (PB1) and 450 nm (PB2) are consistent with the excitonic peak that appeared in the absorption spectra (**Fig. 9a, c**). To evaluate the free exciton dynamics at the FE2 state, the PB2 kinetics under different excitation wavelengths were probed (**Fig. 9d**). A red shift in PB2 observed within 0.5 ps after 315 nm excitation is related to hot carrier (free exciton with high excess energy) relaxation (so-called cooling) processes.[53,54] Under 415-nm excitation, no free excitons are generated at the FE1 state due to the lower excitation energy. That means the TA kinetics of PB2 (red curve in **Fig. 9d**) reflects the intrinsic dynamics of free exciton initially generated at FE2 states. The oscillation in the TA kinetics at an early time (within the first ten ps) is due to the exciton fine structure modulation by coherent optical phonons from the vibrational motion of the $[SnBr_6]^{4-}$ octahedra, which was observed previously in 2D perovskites with a $[PbI_6]^{4-}$ octahedra.[55] To highlight the decaying process of the generated free excitons at FE2 states, the kinetics was fitted with a three-exponential decay, convoluted with a Gaussian function as system response with a FWHM (full width at half maximum) of 150 fs. As can be seen, the photobleaching kinetics decay slowly within the probed time range.

In contrast, under UV excitation at 315 nm, both free excitons and hot carriers at the FE1 state are generated. A red shift in PB2 observed within 0.5 ps after 315 nm excitation is related to hot carrier (free exciton with high excess energy) relaxation (so-called cooling) processes.[54,55] In this regard, at the initial time after excitation (~1 ps) the PB2 kinetics shows a fast decay due to the hot carrier cooling and coherent phonon oscillation. After that, the rise of PB2 kinetic (lasting up to 20 ps) corresponds to the carriers transfer from FE1 states leading to the increased free exciton population at FE2 states. Carriers transfer from PB1 to PB2 states under 315-nm excitation is excluded since their TA kinetics have similar trends (**Fig. 9b**).

Thus, excitation of the samples within PLE bands initiates two processes. Firstly, some of the excited carriers at a hydrated HDA_3SnBr_8 phase states are trapping locally via electron-phonon coupling, forming an STE state, while others are transferring to the 2D $HDASnBr_4$ phase followed by non-radiative recombination and do not contribute to emission. Since the time scales of these processes are different, it is hard to estimate the exact proportion between self-trapped and non-

radiatively decayed excitons. During aging, the 2D $HDASnBr_4$ phase gradually disappears, thereby increasing the probability for free excitons to form self-trapped states. As a result, the ratio between the numbers of emitted and absorbed photons (which PLQY is) increases, resulting in a corresponding increase in the PL intensity and "apparent" PLQY.

In addition, as a final test of the role of humidity in the observed phase transformations and resulting variation in the optical properties, we have exposed the samples to solvent vapor inside the glovebox.[56,57] Recrystallizations and structural transformations have been previously documented for different perovskite materials upon exposure to DMF,[56] alcohol,[57] and water.[58] Thus, as complementary experiments to the effects of exposure humidity, we have exposed samples to DMF and methanol vapor inside the glovebox, and also included a solvent which does not dissolve our perovskite material (toluene) as a control. The obtained results are shown in **Figures S10-S13**. We can see that negligible changes are obtained for exposure to toluene, which does not dissolve the $HDASnBr_4$. In contrast, after the exposure to DMF vapor the samples rapidly turn colorless and luminescence enhances, and then roughness increases (samples turn cloudy and there is significant scattering evident from the absorption spectra). Similar evolution of optical properties is observed for methanol vapor, but it occurs slower which is expected since the solubility of the perovskite in methanol is lower. This is expected as the effect of the solvent on material properties is dependent on the solvent properties.[56] While we can observe clear loss of the 2D phase in the absorption spectra for both DMF and methanol, there is no evidence of 1D phase which forms in ambient in the samples exposed to DMF, while samples exposed to methanol exhibit more similarity to samples in ambient than DMF samples but they all exhibit some differences. From XRD patterns, we can observe no significant changes in the case of toluene. For DMF, the transformation of 2D phase to lower-dimensional phase is clearly visible from the decrease of 00l intensities of $HDASnBr_4$ and appearance of new diffraction lines at 14.77, 15.05, 29.88 and 30.36 ° 2θ. The refinement showed that new crystalline phase is not iso-structural with HDA_3SnBr_8. This, combined with the fact there are no new diffraction lines in low angle range (3-10° 2θ), typical for 2D and 1D perovskites, suggests the transformation 2D phase to 0D perovskite. The same is found for samples exposed to methanol. The only difference is that 2D phase exposed to DMF swiftly transforms to lower dimensional perovskite (within 30 sec), while the new diffraction lines in the case of methanol appear after 8 minutes. Therefore, we can conclude that different solvents can trigger structural transformation due to plasticizing effect of the solvent[57] and/or dissolution/recrystallization.[58] Possible driving force of structural reorganization is different solubility of perovskite precursors in the solvent,[58] which would have a consequence of different solvents resulting in differences in structural transformations observed, consistent with experimental observation.

Conclusions

We investigated ambient stability of $HDASnBr_4$ powders and thin films. We found that the use of additives ($SnCl_2$, TEOS) affected the stability and optical properties of $HDASnBr_4$ due to the changes of phase composition i.e. the ratio of $HDASnBr_4$:hydrated HDA_3SnBr_8 over time. There was no obvious correlation between the luminescence intensity and the Sn^{2+}/Sn^{4+} ratio, and the most intense emission in all samples occurred after ~40 h of ambient exposure, when the samples exhibited comparable amounts of the two phases (although the evolution of the phases over time varied for different additives). Combination of additives results in significant enhancement of the film stability, with luminescence from thin films without any encapsulation observed for over 10 days. The luminescence can be attributed to the emission from the hydrated phase HDA_3SnBr_8, with apparent PLQY increase with aging corresponding to the reduced fraction of the non-emissive 2D $HDASnBr_4$ phase which contributes to non-radiative losses as the FE2 states in 2D phase do not contribute to observable PL.

Experimental methods

Materials. The following chemicals: $SnBr_2$ (TCI, >97.0%), $SnCl_2$ (98%, Alfa Aesar), tetraethyl orthosilicate (TEOS) (99%, Dieckmann), N,N-dimethylformamide (DMF) (anhydrous, Alfa Aesar), Dimethyl sulfoxide (DMSO) (anhydrous, Alfa Aesar), Toluene (anhydrous, Sigma-aldrich, 99.8%) and $HDABr_2$ (Greatcell Solar) were used as purchased without any purification.

Solution preparation. $SnBr_2$ and $HDABr_2$ in a molar ratio of 1:1 were mixed and dissolved in DMF/DMSO (3:1, v/v) to form a clear solution. For the precursors with additives, different amount of $SnCl_2$ and TEOS were added into the $HDASnBr_4$ precursor solution.

Film deposition. The quartz substrates were cleaned by ultra-sonication with detergent solution, deionized water, acetone and ethanol for 20 min, respectively, followed by drying under N_2 flow. After oxygen plasma treatment, substrates were transferred into Ar-filled glovebox for film deposition. The $HDASnBr_4$ perovskite films were spin-coated at spinning speeds of 1000 rpm for 5 s and 5000 rpm for 60 s while 150 µl toluene antisolvent was dropped to facilitate crystallization of perovskites. After that, all films were annealed at 90 ºC for 10 min to remove the residual solvent. Solvent vapor exposure was performed inside the glovebox, by placing the sample in a closed glass Petri dish with solvent droplet of a fixed volume.[56,57]

Characterization. XRD patterns were recorded by Rigaku MiniFlex X-ray Diffractometer using Co Kα radiation. Absorption spectra were measured by Agilent Cary 60 UV-Vis spectrophotometer. PL spectra were measured with HeCd (325 nm) laser as the excitation source, and the spectra were collected by a fiberoptic spectrometer. Top view SEM images were obtained using a LEO 1530FEG Scanning Electron Microscope. Photoluminescence excitation (PLE), quantum yield (PLQY), and decay were measured on an FS5 (Edinburgh Instruments) spectrofluorometer equipped with an integrating sphere. PLE spectra were collected at the emission maximum (λ_{max} = 600 nm) in the 250-550 nm range with a 1 nm step and 2 nm spectral bandwidth. PLQY was determined by the three-measurements technique,[59] wherein, together with measurements of an empty sphere (scatter) and direct excitation of the sample, the PL spectra for indirect excitation (the sample is placed inside a sphere and the excitation beam is directed onto the sphere wall) were collected. The latter accounting for the reabsorption by the sample of the excitation light scattered into the sphere. PL decays were collected under flash-Xe lamp excitation using a multi-channel scaling detection technique. Due to the relatively long time length of the excitation pulse, PL decay traces were first reconvoluted with an instrument response function and then fitted with a monoexponential function (resulting χ^2 value was in a range of 1.1-1.2).

Transient absorption spectroscopy (TAS) was performed on a home-built pump-probe setup with a Ti:Sapphire regenerative amplifier (Coherent Legend Elite) seeded by a titanium sapphire

oscillator (Coherent Mira 900) as a light source. The output of 800 nm at 1 kHz from the amplifier was split into two beams: the first, intensive beam, was set into an optical parametric amplifier (Coherent Opera Solo), providing the pump beam with tunable photon energy; the rest of the laser power was focused on a calcium fluoride plate to generate a supercontinuum probe in 325-700 nm range. The probe beam was passed through a mechanical translation stage, providing a time delay between pump and probe pulses up to 1 ns. The instrumental response function is 150 fs. Shot-by-shot transmission of the probe beam was collected by Acton Spectrapro 275 spectrometer equipped with a 150 ln/mm grating and a line CCD. The differential transmission spectrum of the probe pulse (ΔT/T) was calculated as $((T_{pump}\,ON - T_{pump}\,OFF)/T_{pump}\,OFF)$.

Author Contributions

W. T. S. and Z. X. contributed equally. J. P. and A. B. D. designed the whole study, analyzed and interpreted results and wrote the first draft of the manuscript. W. T. S. prepared the samples and performed PL and XRD characterization. L. M. conducted Le Bail analysis. Y. H. measured XPS spectra, and provided the analysis together with A. M. C. N. PLQY, PLE and transient PL/absorption measurements were performed by Z. X. and A. S., and they also provided analysis of the results together with K.S. W. All authors contributed to the final version of the text.

Conflicts of interest

There are no conflicts to declare.

Acknowledgements

This work was supported by the Seed Funding for Basic Research and Seed Funding for Strategic Interdisciplinary Research Scheme of the University of Hong Kong and RGC GRF projects 17311422 and the PZS-2019-02-2068 project financed by the "Research Cooperability" Program of the Croatian Science Foundation and European Union from the European Social Fund under the Operational Programme Efficient Human Resources 2014-2020.

Notes and references

‡ Footnotes relating to the main text should appear here. These might include

1 Z. Li, Z. Deng, A. Johnston, J. Luo, H. Chen, Y. Dong, R. Sabatini, E. H. Sargent, Precursor Tailoring Enables Alkylammonium Tin Halide Perovskite Phosphors for Solid-State Lighting, *Adv. Funct. Mater.,* 2022, **32**, 2111346

2 X. Zhang, C. Wang, Y. Zhang, X. Zhang, S. Wang, M. Lu, H. Cui, S. V. Kershaw, W. W. Yu, A. L. Rogach, Bright Orange Electroluminescence from Lead-Free Two-Dimensional Perovskites, *ACS Energy Lett.* 2019, **4,** 242.

3 L. Zhang, B. Yang, S. Mei, Y. Zhu, R. Hua, J. Zou, Highly Luminescent Broadband Phosphors based on Acid Solvent Coordinated Two-dimensional Layered Tin-based Perovskites, *J. Mater. Chem. C* 2022, **10**, 3856.

4 I. Poli, G. Kim, E L. Wong, A. Treglia, G. Folpini, A. Petrozza, High External Photoluminescence Quantum Yield in Tin Halide Perovskite Thin Films, *ACS Energy Lett.* 2021, **6**, 609.

5 P. Fu, M. Huang, Y. Shang, N. Yu, H. Zhou, Y. Zhang, S. Chen, J. Gong, Z. Ning, Organic-Inorganic Layered and Hollow Tin Bromide Perovskite with Tunable Broadband Emission, *ACS Appl. Mater. Interfaces* 2018, **10**, 34363.

6 L. Lanzetta, J. M. Marin-Beloqui, I. Sanchez-Molina, D. Ding, S. A. Haque, Two-Dimensional Organic Tin Halide Perovskites with Tunable Visible Emission and Their Use in Light-Emitting Devices, *ACS Energy Lett.* 2017, **2**, 1662.

7 L. Hou, Y. Zhu, J. Zhu, C. Li, Tuning Optical Properties of Lead-Free 2D Tin-Based Perovskites with Carbon Chain Spacers, *J. Phys. Chem. C* **2019**, *123*, 31279.

8 Z. Wang, F. Wang, B. Zhao, S. Qu, T. Hayat, A. Alsaedi, L. Sui, K. Yuan, J. Zhang, Z. Wei, Z. Tan, Efficient Two-Dimensional Tin Halide Perovskite Light-Emitting Diodes via a Spacer Cation Substitution Strategy, *J. Phys. Chem. Lett.* 2020, **11**, 1120.

9 Y Wang, R. Zou, J. Chang, Z. Fu, Y. Cao, L. Zhang, Y. Wei, D. Kong, W. Zou, K. Wen, N. Fan, N. Wang, W. Huang, J. Wang, Tin-Based Multiple Quantum Well Perovskites for Light-Emitting Diodes with Improved Stability, *J. Phys. Chem. Lett.* 2019, **10**, 453.

10 H. Yao, F. Zhou, Z. Li, Z. Ci, L. Ding, Z. Jin, Strategies for Improving the Stability of Tin-Based Perovskite ($ASnX_3$) Solar Cells, *Adv. Sci.* 2020, **7,** 1903540

11 Q. Wei, Y. Ke, Z. Ning, Theoretical Study of Using Kinetics Strategy to Enhance the Stability of Tin Perovskite, *Energy Environ. Mater.* 2020, **3**, 541.

12 A.K. Baranwal, K. Nishimura, D. Liu, M. A. Kamarudin, G. Kapil, S. Saini, T. Yabuki, S. Iikubo, T. Minemoto, K. Yoshino, K. Miyazaki, Q. Shen, S. Hayase, Relationship between Carrier Density and Precursor Solution Stirring for Lead-Free Tin Halide Perovskite Solar Cells Performance, *ACS Appl. Energy Mater*. 2022, **5**, 4002.

13 J. Pascual, D. D. Girolamo, M. A. Flatken, M. H. Aldamasy, G. Li, M. Li, A. Abat, Lights and Shadows of DMSO as Solvent for Tin Halide Perovskites, *Chem. Eur. J.* 2022, **28**, e20210391

14 T. Wang, F. Yan, Reducing Agents for Improving the Stability of Sn-based Perovskite Solar Cells, *Chem. Asian J.* 2020, **15**, 1524.

15 M. Wang, W. Wang, Y. Shen, K. Cao, J. Chen, X. Zhao, M. Xie, S. Chen, Suppression of Sn^{2+} Oxidation and Formation of Large-Size Crystal Grains with Multifunctional Chloride Salt for Perovskite Solar Cell Applications, *J. Mater. Chem. C* 2022, **10**, 10669

16 T. Wu, D. Cui, X. Liu, X. Luo, H. Su, H. Segawa, Y. Zhang, Y. Wang, L. Han, Additive Engineering toward High-Performance Tin Perovskite Solar Cells, *Sol. RRL* 2021, **5**, 2100034.

17 J. Lin, Y. Hu, C. Hou, C. Liao, W. Chuang, C. Chiu, M. Tsai, J. Shyue, P. Chou, Superior Stability and Emission Quantum Yield (23% ¬± 3%) of Single-Layer 2D Tin Perovskite TEA_2SnI_4 via Thiocyanate Passivation, *Small* 2020, **16**, 2000903

18 Q. Tai, X. Guo, G. Tang, P. You, T. Ng, D. Shen, J. Cao, C. Liu, N. Wang, Y. Zhu, C. Lee, F. Yan, Antioxidant Grain Passivation for Air-Stable Tin-Based Perovskite Solar Cells, *Angew. Chem. Int. Ed.* 2019, **58**, 806.

19 Z. Dai, T. Lv, J. Barbaud, W. Tang, T. Wang, L. Qiao, H. Chen, R. Zheng, X. Yang, L. Han, Stable Tin Perovskite Solar Cells Developed via Additive Engineering*, Sci. China Mater.* 2021, **64**, 2645.

20 J. Gong, X. Li, W. Huang, P. Guo, T. J. Marks, R. D. Schaller, T. Xu, Suppressed Oxidation and Photodarkening of Hybrid Tin Iodide Perovskite Achieved with Reductive Organic Small Molecule, ACS Appl. Energy Mater. 2021, **4,** 4704.

21 S. J. Yang, J. Choi, S. Song, C. Park, K. Cho, Enhancing Air-Stability and Reproducibility of Lead-Free Formamidinium-Based Tin Perovskite Solar Cell by Chlorine Doping, *Sol. Energy Mater. Sol. Cells* 2021, **227**, 111072.

22 H. Kim, Y. H. Lee, T. Lyu, J. H. Yoo, T. Park, J. H. Oh, Boosting The Performance and Stability of Quasi-Two-Dimensional Tin-Based Perovskite Solar Cells Using the Formamidinium Thiocyanate Additive, *J. Mater. Chem. A* 2018, **6**, 18173.

23 E. W. Diau, E. Jokar, M. Rameez, Strategies To Improve Performance and Stability for Tin-Based Perovskite Solar Cells, *ACS Energy Lett.* 2019, **4**, 1930.

24 T. Wang, Q. Tai, X. Guo, J. Cao, C. Liu, N. Wang, D. Shen, Y. Zhu, C. Lee, F. Yan, Highly Air-Stable Tin-Based Perovskite Solar Cells through Grain-Surface Protection by Gallic Acid, *ACS Energy Lett*. 2020, **5,** 1741.

25 W. Yang, J. Cao, C. Dong, M. Li, Q. Tian, Z. Wang, L. Liao, Suppressed Oxidation of Tin Perovskite by Catechin for Eco-Friendly Indoor Photovoltaics, *Appl. Phys. Lett.* 2021, **118**, 023501

26 X. Li, J. M. Hoffman, M. G. Kanatzidis, The 2D Halide Perovskite Rulebook: How the Spacer Influences Everything from the Structure to Optoelectronic Device Efficiency, *Chem. Rev*. 2021, **121**, 2230.

27 Y. Guo, M. Sun, W. Yang, S. Yuan, H. Xiong, Z. Tan, J. Fan, W. Li, Enhanced Charge Transport by Regulating the Electronic Structure in 2D Tin-Based Perovskite Solar Cells, *J. Phys. Chem. C* 2022, **126**, 9425.

28 P. Li, X. Liu, Y. Zhang, C. Liang, G. Chen, F. Li, M. Su, G. Xing, X. Tao, Y. Song, Low-Dimensional Dion-Jacobson-Phase Lead-Free Perovskites for High-Performance Photovoltaics with Improved Stability, *Angew. Chem. Int. Ed.* 2020, 59, 6909.

29 Q. Sun, Z. Fang, Y. Zheng, Z. Yang, F. Hu, Y Yang, W. Yang, X. Hou, M. Shang, Regulating the Phase Stability and Bandgap of Quasi-2D Dion-Jacobson $CsSnI_3$ Perovskite via Intercalating Organic Cations, *J. Mater. Chem. A* 2022, **10**, 3996.

30 V. V. Nawale, T. Sheikh, A. Nag, Dual Excitonic Emission in Hybrid 2D Layered Tin Iodide Perovskites, *J. Phys. Chem. C* 2020, **124**, 21129.

31 S. Wang, J. Popović, S. Burazer, A. Portniagin, F. Liu, K. Low, Z.i Duan, Y. Li, Y. Xiong, Y. Zhu, S.V. Kershaw, A. B. DjurišIć, A.L. Rogach, Strongly Luminescent Dion-Jacobson Tin Bromide Perovskite Microcrystals Induced by Molecular Proton Donors Chloroform and Dichloromethane, *Adv. Funct. Mater.* 2021, **31**, 2102182

32 S. Wang, S.V. Kershaw, A.L. Rogach, Bright and Stable Dion-Jacobson Tin Bromide Perovskite Microcrystals Realized by Primary Alcohol Dopants, *Chem. Mater.* 2021, **33**, 5413-5421

33 J. Qi, S. Wang, A. Portniagin, S.V. Kershaw, A.L. Rogach, Room Temperature Fabrication of Stable, Strongly Luminescent Dion-Jacobson Tin Bromide Perovskite Microcrystals Achieved through Use of Primary Alcohols, *Nanomaterials* 2021, **11**, 2738.

34 F. Li, Y. Xie, Y. Hu, M. Long, Y. Zhang, J. Xu, M. Qin, X. Lu, M. Liu, Effects of Alkyl Chain Length on Crystal Growth and Oxidation Process of Two-Dimensional Tin Halide Perovskites, *ACS Energy Lett.* 2020, **5**, 1422.

35 Q. G. Zhang, S. Q. Liu, M. D. He, W. L. Zheng, Q. Wan, M. M. Liu, X. R. Liao, W. J. Zhan, C. W. Yuan, J. Y. Liu, H. J. Xie, X. J. Guo, L. Kong, L. Li, Stable Lead-Free Tin Halide Perovskite with Operational Stability> 1200 h by Suppressing Tin(II) Oxidation, *Angew. Chem. Int. Ed*. 2022, **61**, e202205463.

36 K. P. Marshall, M. Walker, R. I. Walton, R. A. Hatton, Enhanced stability and efficiency in hole-transport-layer-free $CsSnI_3$ perovskite photovoltaics, *Nat. Energy* 2016, **1**, 16178.

37 J. Pascual, M. Flatken, R. FØlix, G. X. Li, S.-H. Turren-Cruz, M. H. Aldamasy, C. Hartmann, M. Li, D. Di Girolamo, G. Nasti, E. Hüsam, R. G. Wilks, A. Dallmann, M. Bär, A. Hoell, A. Abate, Fluoride Chemistry in Tin Halide Perovskites, *Angew. Chem. Int. Ed*. 2021, **60**, 21583–21591.

38 T. Nakamura, T. Handa, R. Murdey, Y. Kanemitsu, A. Wakamiya, Materials Chemistry Approach for Efficient Lead-Free Tin Halide Perovskite Solar Cells, *ACS Appl. Electron. Mater.* 2020, **2**, 3794–3804.

39 T. Nakamura, Shinya Yakumaru, M. A. Truong, K. S. Kim, J. W. Liu, S. F. Hu, K. Otsuka, R. Hashimoto, R. Murdey, T. Sasamori, H. D. Kim, H. Ohkita, T. Handa, Y. Kanemitsu, A. Wakamiya, Sn(IV)-free tin perovskite films realized by in situ Sn(0) nanoparticle treatment of the precursor solution , *Nat. Commun.* 2020, **11**, 3008.

40 B. A. de Carvalho, S. Kavadiya, S. Huang, D. M. Niedzwiedzki, P. Biswas, Highly Stable Perovskite Solar Cells Fabricated Under Humid Ambient Conditions, *IEEE Journal of Photovoltaics* 2017, **7,** 532.

41 Y. L. He, X. Q. Hu, M. X. Xu, A. M. C. Ng, A.B. Djurišić, Mesoporous silica nanosphere-based oxygen scavengers, *Microporous and Mesoporous Materials* 2021, **327**, 111426

42 A. Dučinskas, G. Y. Kim, D. Moia, A. Senocrate, Y. R. Wang, M. A. Hope, A. Mishra, D. J. Kubicki, M. Siczek, W. Bury, T. Schneeberger, L. Emsley, J. V. Milić, J. Maier, M. Grätzel, Unravelling the Behavior of Dion-Jacobson Layered Hybrid Perovskites in Humid Environments, *ACS Energy Lett*. 2021, **6**, 337.

43 S. Ghimire, K. Oldenburg, S. Bartling, R. Lesyuk, C. Klinke, Structural Reconstruction in Lead-Free Two-Dimensional Tin Iodide Perovskites Leading to High Quantum Yield Emission, *ACS Energy Lett.* 2022, **7,** 975.

44 G. A. Mousdis, G. C. Papavassiliou, C. P. Raptopoulou, A. Terzis, Preparation and characterization of $[H_3N(CH_2)_6NH_3]PbI_4$ and similar compounds with a layered perovskite structure. J*. Mater. Chem.* 2000, **10**, 515.

45 S. Joy, H. R. Atapattu, S. Sorensen, H. Pruett, A. B. Olivelli, A. J. Huckaba, A.-F. Miller, K. R. Graham, How additives for tin halide perovskites influence the Sn^{4+} concentration, *J. Mater. Chem. A* 2022, **10**, 13278-13285.

46 Md. E, Kayesh, K. Matsuishi, Ryuji Kaneko, S. Kazaoui, J. J. Lee, T. Noda, A. Islam, Coadditive Engineering with 5-Ammonium Valeric Acid Iodide for Efficient and Stable Sn Perovskite Solar Cells, A*CS Energy Lett.* 2019, **4**, 278-284.

47 B. Turedi, K. J. Lee, I. Dursun, B. Alamer, Z. Wu, E. Alarousu, O. F. Mohammed N. Cho, O. M. Bakr, Water-Induced Dimensionality Reduction in Metal-Halide Perovskites. *J. Phys. Chem. C* 2018, **122**, 14128.

48 X. S. Qin, F. Z. Liu, T. L. Leung, W. T. Sun, C. C. S. Chan, K. S. Wong, L. Kanižaj, J. Popović, A. B. Djurišić, Compositional optimization of mixed cation Dion-Jacobson perovskites for efficient green light emission. J. Mater. Chem. C 2022, 10, 108-114.

49 Z. Xing, Z. Zhou, G. Zhong, *et al*. Barrierless Exciton Self-Trapping and Emission Mechanism in Low-Dimensional Copper Halides. *Adv. Func. Mater.* 2022, **32**, 2207638.

50 J. R. Lakowicz, ed. Principles of fluorescence spectroscopy. 3rd edition. Boston, MA: Springer US, 2006.

51 Q. Wen, S. V. Kershaw, S. Kalytchuk, O. Zhovtiuk, C. Reckmeier, M. I. Vasilevskiy, A. L. Rogach, Impact of D_2O/H_2O Solvent Exchange on the Emission of HgTe and CdTe Quantum Dots: Polaron and Energy Transfer Effects. *ACS Nano* 2016, **10**, 4301.

52 T. Hu, M. D. Smith, E. R. Dohner, M.-J.Sher, M.-J.; Wu, X.; Trinh, M. T.; Fisher, A.; Corbett, J.; Zhu, X. Y.; H. I. Karunadasa, A. M. Lindenberg, Mechanism for Broadband White-Light Emission from Two-Dimensional (110) Hybrid Perovskites. J. Phys. Chem. Lett. 2016, **7**, 2258.

53 J. Fu, Q. Xu, G. Han, B. Wu, C. H. A. Huan, M. L. Leek, T. C. Sum, Hot Carrier Cooling Mechanisms in Halide Perovskites. *Nat. Commun*. 2017, **8**, 1300

54 C. C. S. Chan, K. Fan, H. Wang, Z. Huang, D. Novko, K. Yan, J. Xu, W. C. H. Choy, I. Lončarić, K. S. Wong, Uncovering the Electron-Phonon Interplay and Dynamical Energy-Dissipation Mechanisms of Hot Carriers in Hybrid Lead Halide Perovskites. *Adv. Energy Mater*. 2021, **11**, 2003071
55 J. H. Fu, M. J. Li, A. Solanki, Q. Xu, Y. Lekina, S. Ramesh, Z. X. Shen, T. C. Sum, Electronic States Modulation by Coherent Optical Phonons in 2D Halide Perovskites. *Adv. Mater.* 2021, **33**, 2006233
56 X. J. Sun, C. F. Han, Z. Liu, L. Xu, J. P. Li, H. M. Yu, K.Wang, Effectiveness of Solvent Vapor Annealing on Optoelectronic Properties for Quasi-2D Organic−Inorganic Hybrid Perovskite Light- Emitting Diodes. *J. Phys. Chem. C* 2020, **124**, 28417
57 X. M. Zhao, T. R. Liu, A. B. Kaplan, C. Yao, Y. L. Loo, Accessing Highly Oriented Two-Dimensional Perovskite Films via Solvent-Vapor Annealing for Efficient and Stable Solar Cells. Nano Lett. 2020, 20, 8880
58 B. Turedi, K. J. Lee, I. Dursun, B. Alamer, Z. N. Wu, E. Alarousu, O. F. Mohammed, N. Cho, O. M. Bakr, Water-Induced Dimensionality Reduction in Metal-Halide Perovskites. *J. Phys. Chem. C* 2018, **122**, 14128
59 J. C. de Mello, H. F. Wittmann, R. H. Friend, An Improved Experimental Determination of External Photoluminescence Quantum Efficiency. *Adv. Mater.* 1997, **9**, 230.

Table of Contents

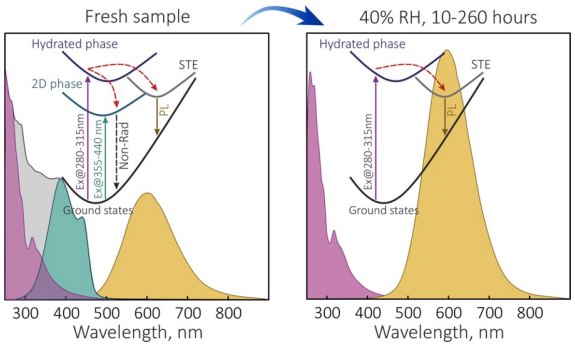

Enhancement of light emission upon ambient exposure in tin-based Dion-Jacobson perovskites occurs due to transformation of non-emissive 2D phase into emissive hydrated 1D phase.